Materials Characterization 128 (2017) 14–22

Contents lists available at ScienceDirect

Materials Characterization

journal homepage: www.elsevier.com/locate/matchar

Evolution of local texture and its effect on mechanical properties and fracture behavior of friction stir welded joint of extruded Mg-3Al-1Zn alloy

Q. Shang [a,b], D.R. Ni [a,*], P. Xue [a], B.L. Xiao [a], Z.Y. Ma [a]

[a] Shenyang National Laboratory for Materials Science, Institute of Metal Research, Chinese Academy of Sciences, 72 Wenhua Road, Shenyang 110016, China
[b] School of Materials Science and Engineering, University of Science and Technology of China, Hefei, China

ARTICLE INFO

Article history:
Received 1 December 2016
Received in revised form 1 March 2017
Accepted 12 March 2017
Available online 14 March 2017

Keywords:
EBSD
Magnesium alloy
Welding
Mechanical property
Texture
Fracture

ABSTRACT

For the wrought Mg alloys, the strong texture may greatly affect their fracture behavior and mechanical property. In the present study, a single plate of extruded AZ31 alloy was subjected to friction stir welding at different tilt angles relative to the extrusion direction, with the aim to investigate the evolution of local texture in the weld as well as its effect on the mechanical behavior of the joint. The results showed that the formation of specific-textured nugget zone and prevalent twinning activated at low strain brought about the reduction of yield anisotropy in the tensile test. Relatively higher elongation of the joints was achieved with the welding direction aligned at 45° to the extrusion direction. The fracture locations were observed to occur in different regions and shift with the variation of the welding direction, which was mainly attributed to the strain localization induced by incompatible deformation of different sub-regions. EBSD analyses indicated that the microstructure and texture evolution in both the nugget zone and the thermo-mechanically affected zone played a vital role in the inconsistent deformation behavior.

1. Introduction

Owing to the superior attributes like high specific strength and stiffness, magnesium alloys, especially high-property wrought alloys, have triggered increasing concern in their structural utilization for weight reduction and energy saving. Recently, along with the rapid development of transport equipment, aviation and aerospace industries, wrought products of profiles and sheets with advanced performance are in great and urgent demand, which brings about growing prominence of joining issues.

As a solid state joining method that can avoid traditional fusion welding defects, friction stir welding (FSW) has been proven appropriate for welding Mg alloys [1–6]. During FSW, frictional heating and severe plastic deformation are introduced to the material by inserting a rotating tool so as to achieve sound joints characterized by fine and equiaxed recrystallized grains [7–9].

For FSW of Mg alloys, the local texture gets evolved in the joints due to the severe material flow driven by the rotating tool and thus would affect the mechanical performance. Although some research suggested that the initial texture does not much affect the final microstructure and texture in the nugget zone (NZ) [3], different texture distributions formed in the thermo-mechanically affected zone (TMAZ) would exert an influence on the mechanical and fracture behavior of the joint as a whole.

In previous studies, FSW Mg alloy joints were reported to show a propensity to fracture close to the interface between NZ and TMAZ [1–4] and the selection of fracture location was generally ascribed to the inconsistent plastic deformation governed by the microstructure and texture differences in neighboring regions [2,4]. Besides, it was also revealed that the initiation and propagation of cracks was correlated with the mechanical twinning [1,2]. Despite these studies, the underline mechanism has not been totally clarified. It is important to figure out the effect of FSW on the detailed microstructure and texture evolution.

Mg sheet products are commonly fabricated by rolling, which is usually time-consuming and costly [10]. Thus, the extrusion process is investigated as an alternative option to produce Mg sheets with flat

Abbreviations: BM, base material; ND, normal direction; STD, transverse direction of extruded sheet; TD, transverse direction of cross-sectional samples; ED, extrusion direction; FSW, friction stir welding; WD, welding direction; NZ, nugget zone; TMAZ, thermo-mechanically affected zone; AS, advancing side; RS, retreating side; UTS, ultimate tensile strength; YS, yield strength; EL, elongation; CRSS, critical resolved shear stress; HAGB, high angle grain boundaries.

* Corresponding author.
E-mail address: drni@imr.ac.cn (D.R. Ni).

http://dx.doi.org/10.1016/j.matchar.2017.03.018
1044-5803/

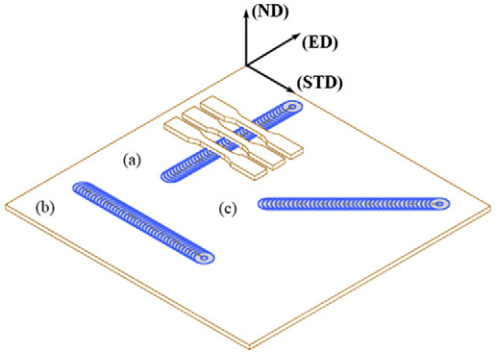

Fig. 1. Schematic illustration of FSW directions aligned at an angle of (a) 0°, (b) 90° and (c) 45° to extrusion direction.

profiles [11–13]. In terms of extruded sheets, unlike rolled sheets and extruded rods, a combination of both rolling and extrusion textures can be obtained, thereby giving rise to pronounced mechanical anisotropy in the sheet plane [11]. Thus, different initial textures can be prepared when extruded Mg alloy sheets are friction stir welded with different tilt angles between the welding direction (WD) and extrusion direction (ED).

In this study, as-extruded AZ31 sheets were subjected to FSW with different WDs relative to the ED to produce different initial textures. The aim of this study is (a) to investigate the general impact of the WD on the microstructure evolution of the joints and (b) to deepen the understanding about the correlation between texture variation and corresponding mechanical behavior.

2. Experimental

As-extruded AZ31 sheets (Mg-3Al-1Zn) with a thickness of 6.4 mm were selected as base material (BM) and welded in three directions aligned at angles of 0°, 45° and 90° to the ED, as illustrated in Fig. 1. Each welding was conducted on a single sheet to eliminate the impact of butting surface, which might introduce some oxide inclusions into the NZ to the disadvantage of analyzing the fracture behavior. A FSW tool with a cylindrical threaded pin 8 mm in diameter and 5.8 mm in length and a concave shoulder 24 mm in diameter was used. The welding was carried out at a speed of 100 mm/min and a rotational rate of 800 rpm.

Optical microscope (OM) and electron backscattered diffraction (EBSD) were used to characterize and analyze the microstructure and the texture variation of the original and the welded Mg alloys. The specimens for OM observation were etched by a solution of 4.2 g picric acid + 70 mL ethanol + 10 mL distilled water + 10 mL glacial acetic acid. The EBSD analysis was conducted by a field emission scanning electron microscope (FESEM, Supra 55) equipped with an EBSD detector and an HKL Channel 5 System.

Vickers hardness and tensile tests were conducted in accordance with ASTM: E384-11e1 and ASTM: E8/E8M-11, respectively. The hardness profiles of the transverse cross-section along the center line of the sheets were examined by a Vickers hardness tester with a 2.94 N load for 10 s. Tensile specimens with a parallel section of 40 × 10 × 6 mm were electrical discharge machined perpendicular to the WD (denoted FSW-0, FSW-45, and FSW-90), and ground with SiC papers up to grit #2000 to achieve a smooth surface. Tensile specimens with the same load direction to the FSW samples were also prepared from original sheets (denoted BM-0, BM-45 and BM-90, correspondingly). All tensile tests were carried out on a Zwick/Roell Z050 tester at a strain rate of 1×10^{-3} s^{-1} at room temperature. Each test was repeated three times.

3. Results

3.1. Microstructure Evolution

Fig. 2 shows the OM microstructure and the grain orientation mapping of the BM. The BM exhibited an inhomogeneous band structures composed of equiaxed fine grains and elongated coarse grains alternately arranged parallel to the sheet plane (Fig. 2a). As characterized by the pole figures (Fig. 2b), a strong basal texture was developed with numerous grains aligning the c-axes parallel to the sheet normal direction (ND) and the c-axes of the remaining grains concentrating close to the sheet transverse direction (STD) with appreciable scatter, which is a typical phenomenon for extruded AZ31 alloy sheets [11]. In the grain orientation map by inverse pole figure (IPF) color-coding (Fig. 2b), it is revealed that the fine grains of similar orientation stringed them together like necklace in the band structure, which could be rationalized by the dynamic recrystallization during extrusion [14].

The transverse cross-sectional macrographs of the FSW AZ31 joints in various directions are shown in Fig. 3. Approximately the same NZ structures in an ellipse-like shape were obtained in the FSW samples with various welding directions. Materials in the TMAZ on both advancing side (AS) and retreating side (RS) exhibited an upwards motion trend with the trace of the band structure bending upwards.

Optical micrographs of the NZ center and the interface of NZ/TMAZ of sample FSW-0 are shown in Fig. 4. It is observed that material in the NZ was completely recrystallized with fine and equiaxed grains. By comparison, the TMAZ underwent incomplete recrystallization with numerous fine grains along with some elongated coarse grains, producing a distinct boundary between NZ and TMAZ. Fig. 5 shows that no apparent differences were discovered in grain size distribution in various regions among the three kinds of samples, implying a feeble correlation between recrystallized grain size and initial texture in FSW.

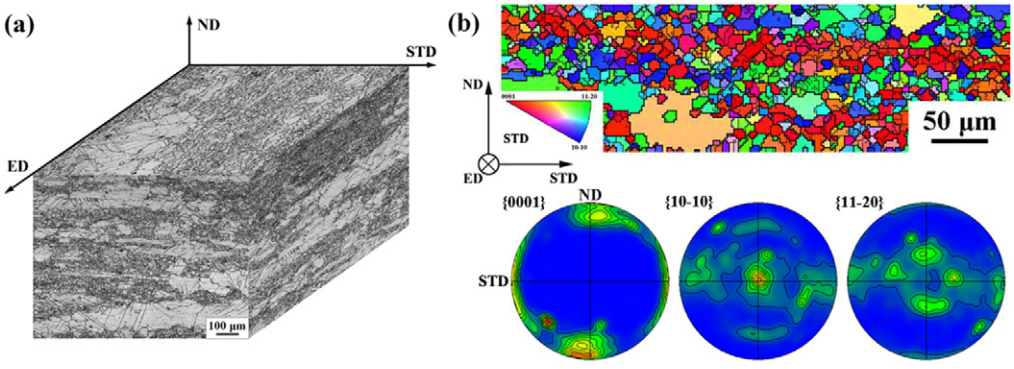

Fig. 2. (a) Optical micrograph, (b) Grain orientation mapping by IPF color-coding (plotted using the STD as reference direction) and pole figures of as-extruded AZ31 sheet.

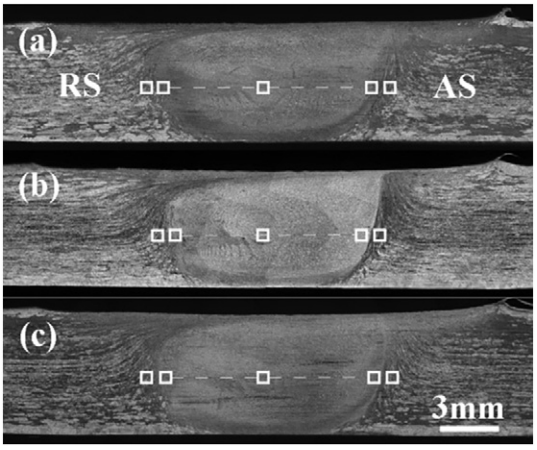

Fig. 3. Macroscopic images of cross-sections of FSW joints: (a) FSW-0, (b) FSW-45, and (c) FSW-90.

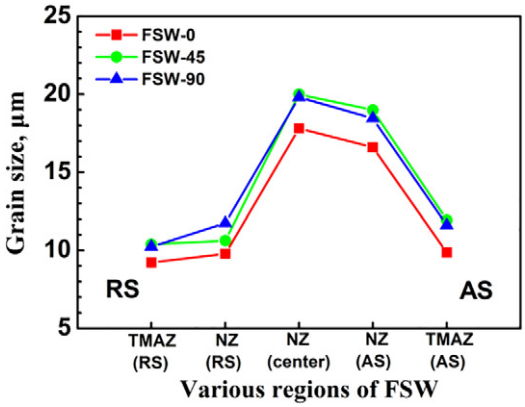

Fig. 5. Recrystallized grain sizes of various regions in samples FSW-0, FSW-45, and FSW-90.

3.2. Texture Evolution

Fig. 6 shows the {0001} pole figures obtained from various regions on the cross sections of three FSW samples. A typical texture distribution was found in the NZ with the (0001) basal planes roughly accumulating along the pin column surface. It is observed that grains near the NZ/TMAZ interface in the NZ aligned their basal planes approximately perpendicular to the transverse direction of the cross-sectional sample (the direction was denoted as TD). The c-axes gradually tilted from TD to WD with the location moving from side to center of NZ. Besides, difference in the grain orientations of the NZ side was found between AS and RS, i.e. the ⟨0001⟩ direction on the AS is inclined a certain degree from the TD to the WD while that on the RS is close to the TD.

Overall, the texture evolved in the NZ is roughly the same among these three kinds of samples, indicating that the initial orientation do not influence the texture modification in the NZ. However, the texture evolution in the TMAZ varied with different initial textures and the texture intensity was drastically weakened compared with that in the NZ.

3.3. Mechanical Behavior

Fig. 7 presents the engineering stress-strain curves of both the BM and FSW joints in various tensile directions and Table 1 summarizes the tensile properties. It is seen that no apparent difference in ultimate tensile strength (UTS) is observed while noticeable yield anisotropy is displayed in the BM. The highest yield strength (YS) is obtained when the loading direction is along the ED and it decreased rapidly with the specimen tilting towards the TD. At a tilt angle of 45°, the FSW joint shows a medium YS and a distinctively higher elongation.

The tensile properties of the FSW joints are bound to change compared with the initial sheets due to significant microstructure evolutions. From the stress-strain curves and tensile properties presented in Fig. 7b and Table 1, it is clear that the YS of all three kinds of samples was reduced after FSW. Additionally, microstructural heterogeneity led to a massive decrease in the elongation of all samples, though the elongation of sample FSW-45 was still higher than that of samples FSW-0 and FSW-90.

The micro hardness profile measured along the mid-thickness on the cross sections of the FSW joints is shown in Fig. 8. It is found that the hardness values fluctuated between 55 and 70 HV in various regions with a general regularity observed in the NZ. It is revealed that the NZ center exhibited a relatively high hardness. With the increase of distance from the NZ center to the TMAZ on the AS, the hardness gradually decreased and finally reached the lowest value approximately at the NZ/TMAZ interface, similar with previous investigation [15]. On the RS, the peak hardness is obtained near the NZ/TMAZ interface and the region with the lowest hardness is located between the NZ center and the boundary.

3.4. Fracture Behavior

Fig. 9 shows the macroscopic images of the failed samples. During transverse tensile test, non-uniform deformation was observed in the NZ with the surface appearance differed between the two sides of the specimen. It is noted that on the plane where the pin passed later (denoted Plane A, Fig. 9a), the NZ center protruded to the WD and the regions in the NZ adjacent to the two NZ/TMAZ interfaces exhibited a significant shrinkage while unconspicuous irregularity was displayed on another plane (denoted Plane B, Fig. 9a). The fracture location on Plane A occurred at the regions with obvious thickness reduction or necking and the crack propagation path tortured to the NZ center on Plane B.

Two types of fracture modes were found in the transverse tensile samples, as displayed in Fig. 9b. It is observed that the fracture locations on Plane A can appear on both AS and RS. Cracking on the AS usually occurred close to the NZ/TMAZ interface while the fracture on the RS exhibited a deviation of about 2 mm from the interface. Specifically,

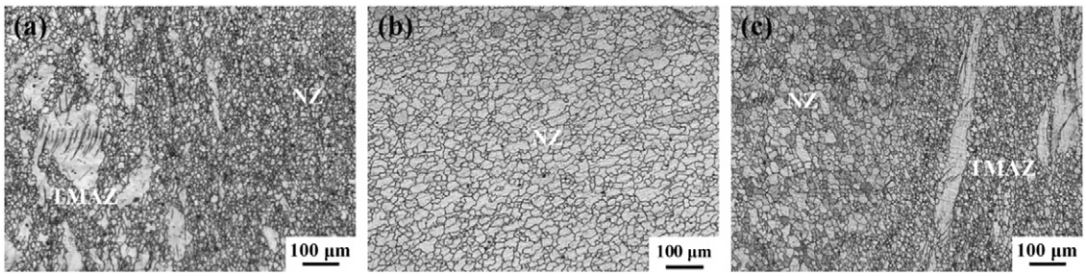

Fig. 4. Optical micrographs of sample FSW-0: (a) NZ/TMAZ interface on RS, (b) NZ center, (c) NZ/TMAZ interface on AS.

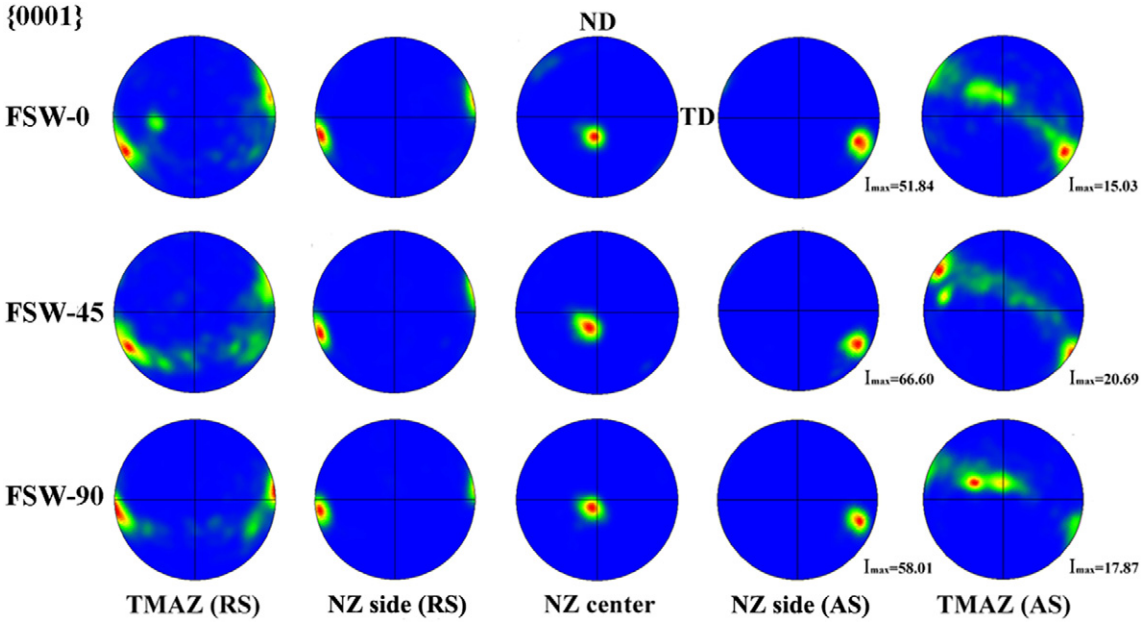

Fig. 6. {0001} pole figures of various positions on transverse cross-sections of FSW joints. (The measurement places are indicated in Fig. 3).

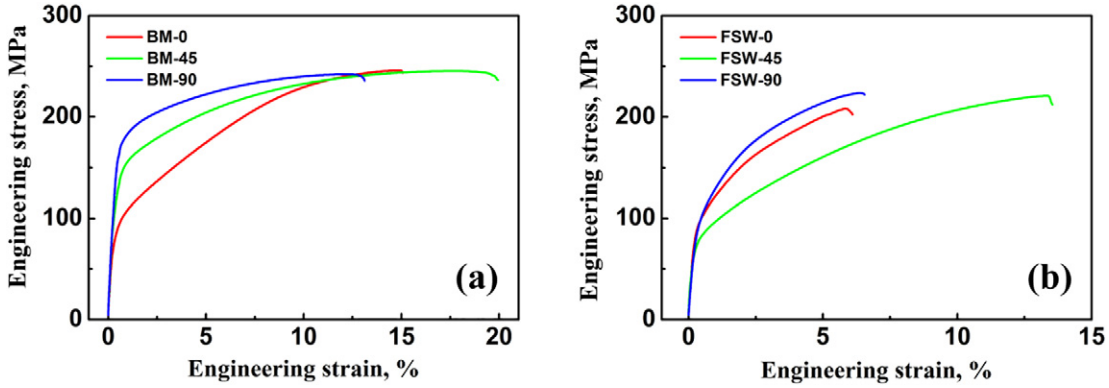

Fig. 7. Tensile engineering stress vs engineering strain curves of (a) base material and (b) FSW joints at an angle of 0°, 45°, and 90° to extrusion direction.

sample FSW-0 tended to crack on the RS while the fractures of samples FSW-45 and FSW-90 were more likely to initiate from the AS, which will be further discussed in subsequent part.

4. Discussion

4.1. Microstructure Evolution

In the FSW process, the heating is generated by the friction between the tool and the workpiece and the plastic deformation of workpiece. With a certain set of welding parameters, the BMs with different initial textures would undergo dynamic recrystallization induced by approximately the same thermal and mechanical effect from the tool, thus achieving similar NZ structures.

As for the upward bending of band structures in the TMAZ, it could be attributed to the transverse squeeze in the plate from the rotating pin and consequent upward material flow to fill the space under the concave shoulder during FSW, which might determine the resultantly evolved texture in the TMAZ from original state.

4.2. Texture Evolution

In terms of texture evolution in the NZ, it is noted that the formation of the special texture distribution should be related to the specific mode of material flow imposed by the rotating tool. It was reported by Krishnan [16] that the FSW process can be simply considered as an extrusion process, i.e. extruding one semi-circular layer in one rotation of the tool. Park et al. [17] found that the repetitive stacking of these shear

Table 1
Tensile properties of as-extruded AZ31 sheet and FSW joints.

Tensile properties	BM-0	BM-45	BM-90	FSW-0	FSW-45	FSW-90
YS, MPa	91.7 ± 7.0	130.1 ± 3.4	158.4 ± 5.0	91.7 ± 3.7	69.7 ± 1.7	95.8 ± 6.4
UTS, MPa	242.5 ± 3.4	244.0 ± 1.2	243.1 ± 2.6	211.3 ± 2.8	220.6 ± 0.3	223.7 ± 0.4
Elongation, %	15.0 ± 0.6	19.9 ± 0.5	12.8 ± 0.9	7.4 ± 1.5	13.8 ± 0.5	7.3 ± 1.1
Joint efficiency, %				87.1	90.4	92.0

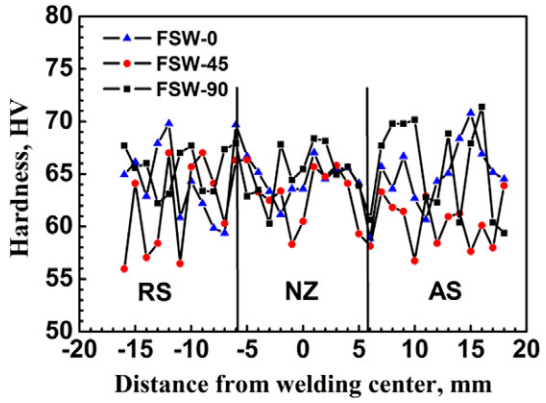

Fig. 8. Cross-sectional hardness profiles of FSW joints along mid-thickness.

layers would lead to the formation of a strong texture with basal planes roughly aligning with the semi-layers. As for the distinct asymmetry of grain orientation observed in the NZ, it could be concerned with the discrepancy found in flow patterns and temperature distribution between AS and RS during FSW [18–20].

As illustrated in Fig. 10, there is a great difference in crystalline orientation between the NZ side (final texture state) and the BM (original texture state). As the transitional region that has also experienced plastic deformation, the TMAZ actually plays a vital role in texture transformation from the BM texture to the NZ texture. In comparison between the schematics of BM orientations and the TMAZ texture shown in Fig. 10, it can be inferred that approximately all the texture components with basal planes perpendicular to the ND were removed in the formation process of TMAZ texture, which deserves detailed analysis.

The TMAZ near the undeformed regions is shown in Fig. 11. In the map, extension twins were activated with twin boundaries substantially parallel to the nearby fine-grain bands, indicating some latent connection between twinning and formation of fine grain bands. As shown in Fig. 11b, the boundaries of twin-like structure are composed of both high angle grain boundaries (HAGBs) and $\{10\bar{1}2\}$ twin boundaries with exact misorientation of about 86°, demonstrating the transformation from twin boundaries into random HAGBs to accommodate plastic strain. Concurrently, dynamic recrystallization was observed along the twin boundaries, consistent with the regarding report [21] that twins can serve as a nucleation site for providing HAGBs. Thus, the formation of band structures with equiaxed fine grains might originate from the development of twin boundaries and relevant recrystallization. Similar deduction has been made by Mironov et al. [22] in the study of microstructure evolution during FSW of AZ31.

From the shear direction of twins and the induced orientation evolution, it can be deduced that the material in the TMAZ has experienced the transverse squeeze originating from the motion of pin. Thus, the almost complete disappearance of texture components with the c-axis close to the ND can be attributed to extension twinning, which gave rise to a reorientation of (0001) basal planes nearly parallel to the ND.

In close proximity to the NZ boundaries (Fig. 12), the gradual transition of grain orientations can also reflect the contribution of twinning. With increased access to the interface, the amount of grains with the c-axes near the WD gradually decreases while grains with the c-axes close to the TD of sample gradually increase. The orientation relationship between these two groups of grains is found to be fairly in accordance with that expected for $\{10\,\bar{1}\,2\}$ twinning. This reveals the growing effect of twinning involved in the microstructure evolution when approaching the NZ boundary, which can be attributed to the continuous increase in strain imposed by FSW at region closer to the rotating pin.

Conclusively, twinning plays an important role in the microstructure and texture evolution process of TMAZ, which involves several stages. Firstly, preliminary twinning occurs to reorient grains by aligning the c-axes roughly parallel with the sheet plane. Subsequently, twinning continuously takes place to drive basal planes parallel to the NZ boundary. In the formation process of TMAZ, twinning process is simultaneously accompanied by the dynamic recrystallization and slip. Additionally, the materials in the TMAZ will undergo increasing plastic strain with the location approaching to the NZ.

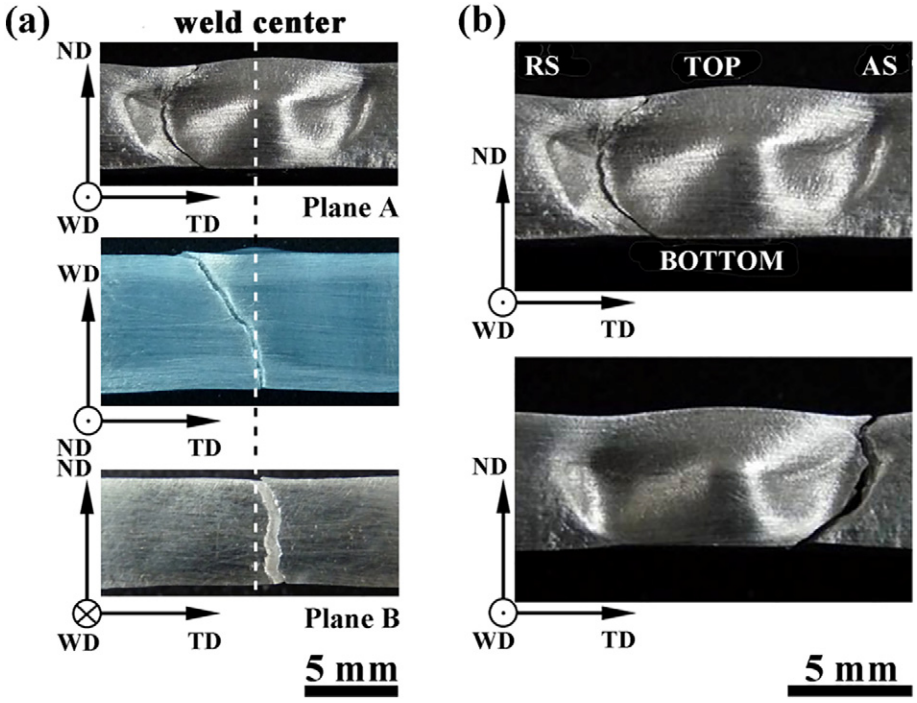

Fig. 9. Macroscopic images of failed FSW joints showing: (a) specific crack propagation path, (b) two possible fracture locations.

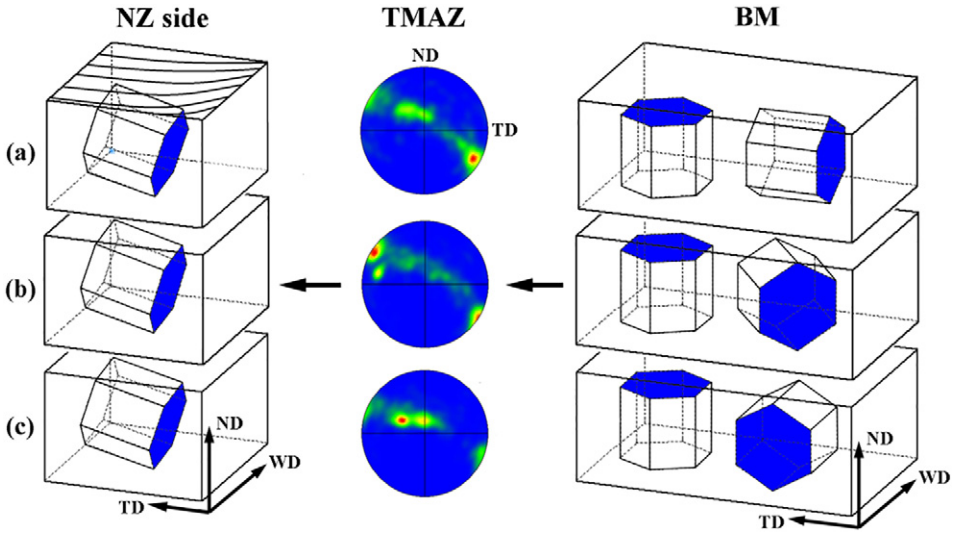

Fig. 10. Schematic of variation in crystalline orientation in various regions of FSW joints on AS: (a) FSW-0, (b) FSW-45, (c) FSW-90.

4.3. Mechanical Properties

As shown in Fig. 7a, distinct yield anisotropy is observed in the original sheets. This orientation-dependence of mechanical behavior can be explained by the different plastic deformation modes prevalent in tension. The (0001) pole figures of BM (Fig. 2b) indicates the extremely hard orientation for both basal slip and extension twinning in sample BM-90 as basal planes parallel to the tensile direction. The stress required for yielding can thus be enhanced as the critical resolved shear stress (CRSS) for the non-basal slip is much higher than that for the basal slip [23].

For sample BM-0, the texture component with the basal planes perpendicular to the tensile direction can give rise to the prevalent activation of extension twinning at a low strain. Barnett et al. [24] reported that approximately 45 pct of deformation can be attributed to extension twinning in the yielding of extruded AZ31 with the maximum Schmid factor. As the CRSS for the $\{10\bar{1}2\}\langle 10\bar{1}1\rangle$ extension twinning is just 2–4 MPa [25], the resultant yield stress would be relatively low.

In terms of sample BM-45, numerous grains are in favorable orientation for the basal slip and the twinning reorients the basal plane nearly 90° to another appropriate alignment. Well operation of both basal slip and twinning contributes to the uniform deformation and improved elongation.

As for the FSW joints, there is no significant difference in YS, which is apparently in association with the introduction of the similar NZ structures among the three kinds of joints. It is confirmed that the finally developed texture in the NZ after FSW reorients the grains near the NZ boundary with a strong tendency to align (0001) basal plane perpendicular to the loading direction. Thus, extension twinning is expected to generate preferentially on both sides of the NZ/TMAZ interface, especially on the RS due to its favorable grain orientation. Appropriate orientation as well as the low CRSS facilitates the mass multiplication of extension twinning near the NZ boundaries at a low strain, which contributes to the yield process of joints. As demonstrated in Fig. 13, the twinning initiated close to the NZ/TMAZ interface of sample FSW-0, when the sample was just to yield under a stress of about 100 MPa during tension.

Besides, Commin et al. [19,26] confirmed that the residual stress actually acted as a prevailing factor in the yield stress of FSW AZ31 and also found that high residual stress could be induced by the formation of microstructure gradient and free stress strains generated.

Thus, the early occurrence of yielding in sample FSW-45 could be explained by its lower residual stress compared with that of sample FSW-0

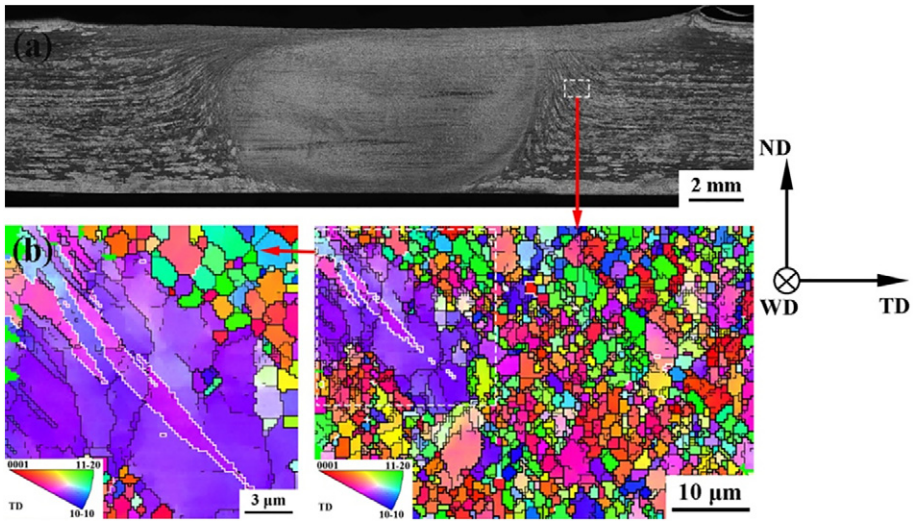

Fig. 11. Microstructure of TMAZ in sample FSW-90: (a) macroscopic image, (b) IPF images.

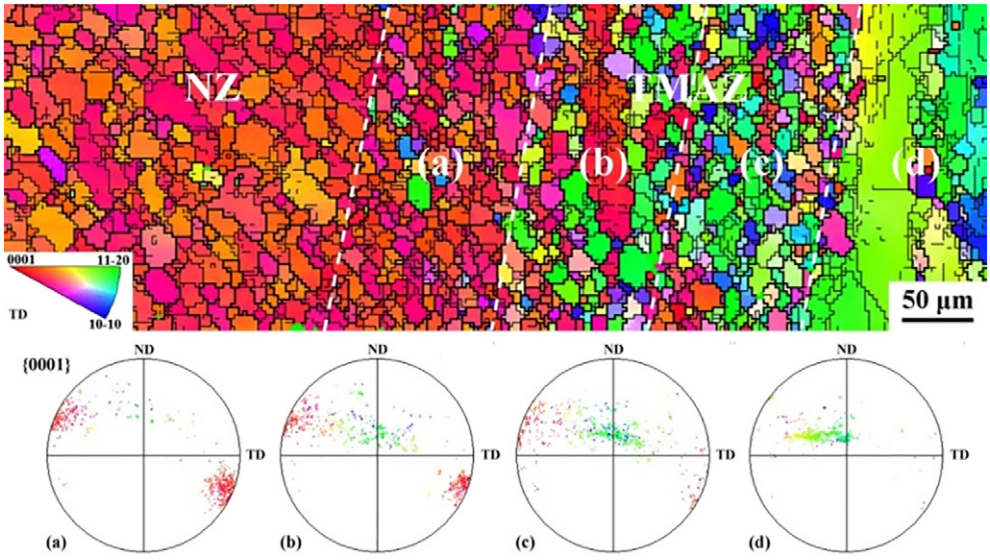

Fig. 12. Gradual texture variation in TMAZ with approaching NZ boundary (sample FSW-90).

and FSW-90, owing to the well mechanical accommodation between different sub-regions across the weld of FSW-45.

In order to verify the contribution of different sub-regions to the overall ductility, the gauge length of 40 mm was equally divided into 8 parts and the elongation of each part was measured respectively. As illustrated in Fig. 14, distinct difference in elongation of various regions reveals the concentration of plastic deformation at the NZ and adjacent regions. In contrast with samples FSW-0 and FSW-90, both NZ and non-NZ regions in sample FSW-45 exhibit considerably better elongations and thereby contribute to the entire performance. The obviously improved elongation in the NZ of sample FSW-45 might be attributed to the constrained strain localization owing to the accommodation of non-NZ regions.

Besides, drastic decrease of elongation was observed between NZ and TMAZ on the AS in both samples FSW-45 and FSW-90, demonstrating severe inconsistency in deformation capability among these regions. This deformation incompatibility among various sub-regions is associated with the microstructure and texture evolution after FSW. The texture variation in different regions endows the grains with hard or soft orientations, and hence gives rise to different performances in plastic deformation.

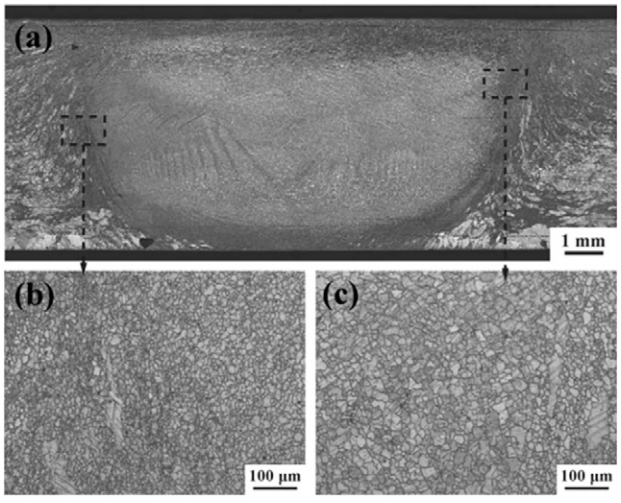

Fig. 13. Profuse initiation of twinning near NZ/TMAZ boundaries in sample FSW-0 when tension was performed up to a stress level of about 100 MPa.

As revealed in Fig. 10, in the NZ-side region on the AS, basal slip is relatively easy to active while the orientation of BM in samples FSW-0 and FSW-90 is quite hard for basal slip, which is consistent with the result in Fig. 14. Compared with the BM, the elongation of TMAZ in all three kinds of FSW samples is enhanced to an extent due to the texture evolution from the original BM texture. As seen in Fig. 6, (0001) basal planes in the TMAZs (AS) of three kinds of samples are all aligned in a rotation around an axis which inclines about 30° with the ND, but the locations of poles with max intensity are different. Specifically, the texture of TMAZ in sample FSW-90 would be the hardest for basal slip while that in sample FSW-45 would be the softest among the three kinds of samples, also agreeing well with the results in Fig. 14.

4.4. Fracture Mechanism

As illustrated in Fig. 9, the fracture on Plane A could occur on the AS or the RS. The cracking on the AS was roughly along the NZ boundary while the fracture on the RS was shifted for a certain distance from the NZ boundary to the NZ center. Intuitively, the fracture locations

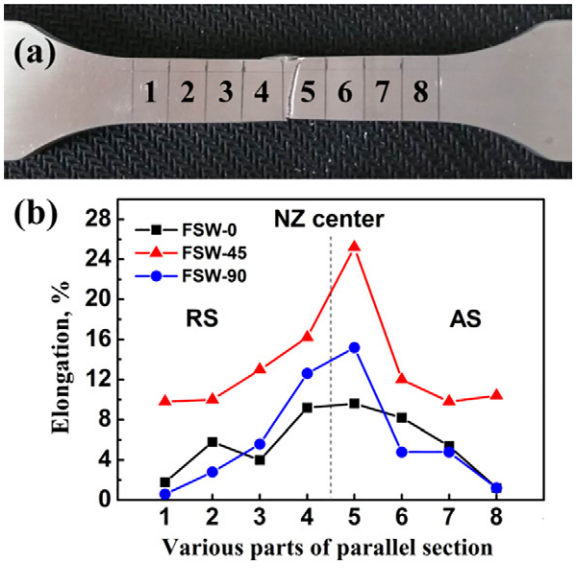

Fig. 14. (a) Schematic illustration of partition of gauge length and (b) elongations of corresponding sub-regions.

agree well with the two low hardness points in the NZ (Fig. 8). Among various factors like grain size, dislocation density, second phase etc. that influence hardness, crystalline orientation actually plays an important role in microhardness performance of Mg alloys, especially like AZ31 which is low-alloyed with limited number of second phase particles.

For FSW Mg-Al-Zn alloys, Yang et al. [1] and Park et al. [27] found the absence of significant differences in the dislocation density throughout the weld via TEM characterization. Furthermore, it was reported by Chang et al. [28] and Wang et al. [29] that the hardness and YS values of FSW AZ31 were insensitive to grain size variation. Consequently, the effect of grain size and dislocation density on microhardness distribution is significantly weakened by the comparatively uniform microstructure obtained in the NZ in this study, highlighting the prominent contribution of grain orientation to the hardness value.

Moreover, the microhardness characterization on the cross-sections, in principle, can endow transverse tension stress to specific micro-regions as the hardness testing is an indentation process perpendicular to the cross-sectional surface, imposing compression along the WD on local grains. Hence, the microhardness measuring can actually provide a site specific visualization of local transverse extension deformability to some extent. As a result, it is implied that sub-regions with the lowest hardness possess the softest crystal orientation for transverse tensile deformation, thereby causing the strain localization and subsequent crack initiation at such places.

Due to the dominant contribution of basal slip to plastic deformation at room temperature [30–31], the softest sub-regions with the lowest hardness in the NZ usually exhibit a strong texture with basal planes at about 45° from the tensile direction. According to the texture distribution in the NZ (Fig. 6), there should be two sub-regions with the softest orientation. One is close to the NZ boundary on the AS and another locates between the NZ center and the NZ boundary on the RS due to the texture asymmetry in the NZ. This is considered as the reason for the difference in fracture location between AS and RS.

As for the propensity of the three kinds of FSW samples in selection of fracture location, it can be ascribed to the deformation inconsistency shown in Fig. 14. The abrupt change in elongation between the NZ and the TMAZ on the AS for samples FSW-45 and FSW-90 indicates that plastic deformation concentrates at the NZ near the boundaries and hence induces obvious necking, which can modify the local stress state by introducing three-dimensional stress and sequentially accelerate the crack initiation. For sample FSW-0, there is no sudden change in elongation across the NZ boundary on the AS so that the cracking tends to occur on the RS and the fracture can also be attributed to the strain localization induced by the poor deformability of adjacent regions.

It is found in Fig. 6 that the grains near the NZ center were oriented unfavorably for both basal slip and extension twinning while those close to the NZ boundary on the RS were quite appropriate for extension twinning rather than the basal slip. In case of tension along the c-axis, the basal plane is reoriented nearly 90° by twinning from one hard orientation to another. Therefore, deformation rapidly concentrates in the region between the NZ center and the boundary on the RS, thus inducing the crack initiation.

As shown in Fig. 9, the crack propagation path usually deflected to the NZ center from Plane A to Plane B, which is believed to be potentially correlated with the formation of $\{10\bar{1}1\}$ contraction twinning, which is expected to activate as the c-axis is compressed. As exhibited in Fig. 15, plenty of needle-like twins with straight smooth boundaries could be detected in the NZ center of sample FSW-0 stretched to 190 MPa, nearly 90% of the UTS. According to the texture distribution, the grains in the NZ center align their basal planes perpendicular to the WD, displaying a favorable orientation for contraction twinning as the basal planes are in compression when the samples are subject to transverse tension. Accordingly, these twins can be considered to be contraction twins due to their typical morphology and orientation characteristic illustrated in Fig. 15.

It was reported that the contraction twinning and its secondary twinning may be responsible for the premature failure of Mg alloys in a macroscopically brittle manner with little area reduction [32–33]. The formation of these twins with the lattice reoriented to be favorable for the basal slip could produce localized shear deformation within them and then induce the local generation of twin sized voids [34], exerting a great influence on the fracture behavior. In this study, the crack initiated on Plane A firstly grew towards the NZ center along the

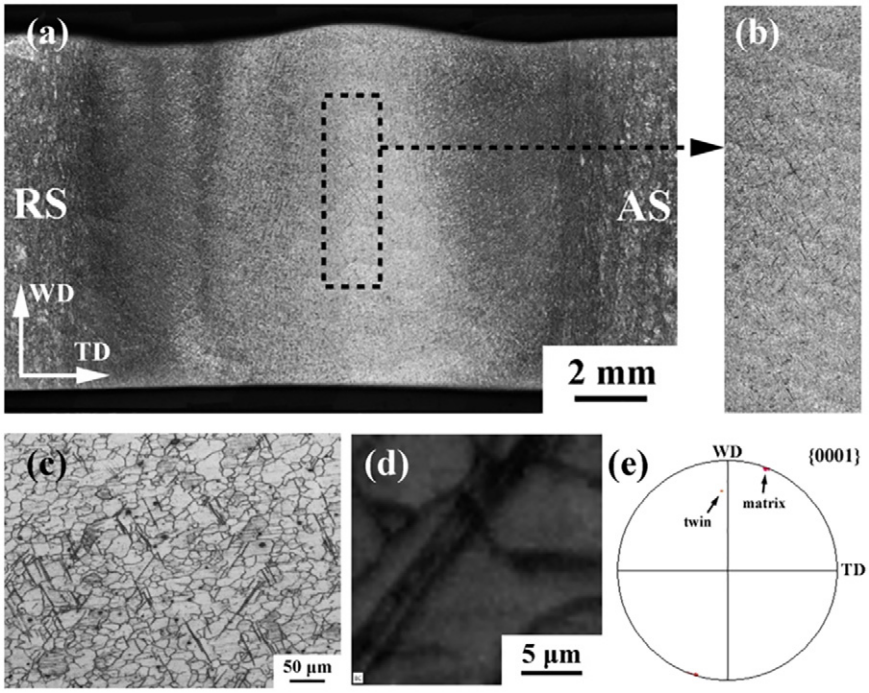

Fig. 15. Characterization of contraction twinning in NZ center of sample FSW-0 under tensile stress of 190 MPa: (a) macroscopic image of horizontal cross-section, (b) distribution area, (c) optical microstructure, (d) Kikuchi band contrast and (e) basal pole figure showing orientation relationship expected for $\{10\bar{1}1\}$–$\{10\bar{1}2\}$ double twin boundaries ($38°\langle 11\bar{2}0\rangle \pm 5°$).

trace of basal plane as the cleavage was along basal plane. Then, the crack path was altered to along the WD when encountering numerous twin sized voids formed in the NZ center, despite the fact that local alignment of basal planes is actually inappropriate for such propagation direction without contraction twinning.

Wonsiewi et al. [35] reported that the average value of CRSS for the contraction twinning is about 112 MPa, which is much higher than that for the extension twinning (2–4 MPa). Thus, unlike the extension twins initiated near the NZ boundaries at a low strain, the contraction twins in the NZ center could just be activated at a high tensile stress and lead to rapid failure before long.

5. Conclusions

In this study, extruded AZ31 plates were friction stir welded with different tilt angles relative to the extrusion direction to investigate the microstructure and texture evolution and associated effect on mechanical properties and fracture behavior. Several conclusions made from this work are as follows.

(1) The extension twinning and accompanied dynamic recrystallization play an important role in the formation process of the final microstructure and texture in the TMAZ.
(2) Similar UTS was obtained for joints with different welding directions, achieving a joint efficiency of about 90%.
(3) At a tilt angle of 45° between welding direction and extrusion direction, significantly higher elongation of the joint was obtained, which can be explained by the reduced strain localization owing to the accommodation of well-deformable non-NZ regions.
(4) The three FSW samples exhibited similar hardness profiles along mid-thickness of the sheets with two highs and two lows in the NZ. The whole variation trend of hardness in the NZ showed some of texture dependence.
(5) The fracture locations on Plane A were in accordance with the lowest hardness points in the NZ, at which the local texture was deduced to be favorable for basal slip. The fracture locations of FSW samples shifted with the three welding directions, which can be attributed to the incompatible deformation of different sub-regions. Contraction twins generated at the NZ center exerted an effect on crack propagation.

Acknowledgement

This work was supported by the National Natural Science Foundation of China under Grant Nos. 51371179 and 51331008.

References

[1] J. Yang, B.L. Xiao, D. Wang, Z.Y. Ma, Effects of heat input on tensile properties and fracture behavior of friction stir welded Mg–3Al–1Zn alloy, Mater. Sci. Eng. A 527 (2010) 708–714.
[2] R.L. Xin, B. Li, A.L. Liao, Z. Zhou, Q. Liu, Correlation between texture variation and transverse tensile behavior of friction-stir-processed AZ31 Mg alloy, Metall. Mater. Trans. A 43A (2012) 2500–2508.
[3] R.L. Xin, D.J. Liu, B. Li, L.Y. Sun, Z. Zhou, Q. Liu, Mechanisms of fracture and inhomogeneous deformation on transverse tensile test of friction-stir-processed AZ31 Mg alloy, Mater. Sci. Eng. A 565 (2013) 333–341.
[4] J. Yang, D. Wang, B.L. Xiao, D.R. Ni, Z.Y. Ma, Effects of rotation rates on microstructure, mechanical properties, and fracture behavior of friction stir-welded (FSW) AZ31 magnesium alloy, Metall. Mater. Trans. A 44A (2013) 517–530.
[5] R.Z. Xu, D.R. Ni, Q. Yang, C.Z. Liu, Z.Y. Ma, Pinless friction stir spot welding of Mg-3Al-1Zn alloy with Zn interlayer, J. Mater. Sci. Technol. 32 (2016) 76–88.
[6] W.Y. Li, T. Fu, L. Hütsch, J. Hilgert, F.F. Wang, J.F. dos Santos, N. Huber, Effects of tool rotational and welding speed on microstructure and mechanical properties of bobbin-tool friction-stir welded Mg AZ31, Mater. Des. 64 (2014) 714–720.
[7] R.S. Mishra, Z.Y. Ma, Friction stir welding and processing, Mater. Sci. Eng. R 50 (2005) 1–78.
[8] Z.Y. Ma, Friction stir processing technology: a review, Metall. Mater. Trans. A 39A (2008) 642–658.
[9] E.A. El-Danaf, M.M. El-Rayes, M.S. Soliman, Friction stir processing: an effective technique to refine grain structure and enhance ductility, Mater. Des. 31 (2010) 1231–1236.
[10] M.R. Barnett, M.D. Nave, C.J. Bettles, Deformation microstructures and textures of some cold rolled Mg alloys, Mater. Sci. Eng. A 386 (2004) 205–211.
[11] S. Gall, R.S. Coelho, S. Muller, W. Reimers, Mechanical properties and forming behavior of extruded AZ31 and ME21 magnesium alloy sheets, Mater. Sci. Eng. A 579 (2013) 180–187.
[12] S. Gall, S. Muller, W. Reimers, Microstructure and mechanical properties of magnesium AZ31 sheets produced by extrusion, Int. J. Mater. Form. 6 (2013) 187–197.
[13] J.R. Dong, D.F. Zhang, J. Sun, Q.W. Dai, F.S. Pan, Effects of different stretching routes on microstructure and mechanical properties of AZ31B magnesium alloy sheets, J. Mater. Sci. Technol. 31 (2015) 935–940.
[14] M.A. Azeem, A. Tewari, S. Mishra, S. Gollapudi, U. Ramamurty, Development of novel grain morphology during hot extrusion of magnesium AZ21 alloy, Acta Mater. 58 (2010) 1495–1502.
[15] N. Afrin, D.L. Chen, X. Cao, M. Jahazi, Microstructure and tensile properties of friction stir welded AZ31B magnesium alloy, Mater. Sci. Eng. A 472 (2008) 179–186.
[16] K.N. Krishnan, On the formation of onion rings in friction stir welds, Mater. Sci. Eng. A327 (2002) 246–251.
[17] S.H.C. Park, Y.S. Sato, H. Kokawa, Basal plane texture and flow pattern in friction stir weld of a magnesium alloy, Metall. Mater. Trans. A 34A (2003) 987–994.
[18] A.N. Albakri, B. Mansoor, H. Nassar, M.K. Khraisheh, Thermo-mechanical and metallurgical aspects in friction stir processing of AZ31 Mg alloy–a numerical and experimental investigation, J. Mater. Process. Technol. 213 (2013) 279–290.
[19] L. Commin, M. Dumont, J.-E. Masse, L. Barrallier, Friction stir welding of AZ31 magnesium alloy rolled sheets: influence of processing parameters, Acta Mater. 57 (2009) 326–334.
[20] J.A. Schneider, A.C. Nunes, Characterization of plastic flow and resulting microtextures in a friction stir weld, Metall. Mater. Trans. B Process Metall. Mater. Process. Sci. 35 (2004) 777–783.
[21] E. Popova, A.P. Brahme, Y. Staraselski, S.R. Agnew, R.K. Mishra, K. Inal, Effect of extension {1012} twins on texture evolution at elevated temperature deformation accompanied by dynamic recrystallization, Mater. Des. 96 (2016) 446–457.
[22] S. Mironov, T. Onuma, Y.S. Sato, H. Kokawa, Microstructure evolution during friction-stir welding of AZ31 magnesium alloy, Acta Mater. 100 (2015) 301–312.
[23] H. Yoshinaga, R. Horiuchi, On nonbasal slip in magnesium crystals, Trans. JIM 5 (1964) 14–21.
[24] M.R. Barnett, A. Ghaderi, J.D. Robson, Contribution of twinning to low strain deformation in a Mg alloy, Metall. Mater. Trans. A 45 (2013) 3213–3221.
[25] R.E. Reedhill, W.D. Robertson, Additional modes of deformation twinning in magnesium, Acta Metall. 5 (1957) 717–727.
[26] L. Commin, M. Dumont, R. Rotinat, F. Pierron, J.-E. Masse, L. Barrallier, Influence of the microstructural changes and induced residual stresses on tensile properties of wrought magnesium alloy friction stir welds, Mater. Sci. Eng. A 551 (2012) 288–292.
[27] S.H.C. Park, Y.S. Sato, H. Kokawa, Effect of micro-texture on fracture location in friction stir weld of Mg alloy AZ61 during tensile test, Scr. Mater. 49 (2003) 161–166.
[28] C.I. Chang, C.J. Lee, J.C. Huang, Relationship between grain size and Zener–Holloman parameter during friction stir processing in AZ31 Mg alloys, Scr. Mater. 51 (2004) 509–514.
[29] Y.N. Wang, C.I. Chang, C.J. Lee, H.K. Lin, J.C. Huang, Texture and weak grain size dependence in friction stir processed Mg–Al–Zn alloy, Scr. Mater. 55 (2006) 637–640.
[30] T. Obara, H. Yoshinga, S. Morozumi, {11$\bar{2}$2} ⟨11$\bar{2}$3⟩ slip system in magnesium, Acta Metall. 21 (1973) 845–853.
[31] J.F. Stohr, J.P. Poirier, Electron-microscope study of pyramidal slip {11$\bar{2}$2} ⟨11$\bar{2}$3⟩ in magnesium, Philos. Mag. 25 (1972) 1313–1329.
[32] D. Ando, J. Koike, Y. Sutou, The role of deformation twinning in the fracture behavior and mechanism of basal textured magnesium alloys, Mater. Sci. Eng. A 600 (2014) 145–152.
[33] P. Cizek, M.R. Barnett, Characteristics of the contraction twins formed close to the fracture surface in Mg–3Al–1Zn alloy deformed in tension, Scr. Mater. 59 (2008) 959–962.
[34] M.R. Barnett, Twinning and the ductility of magnesium alloys part II. “Contraction” twins, Mater. Sci. Eng. A 464 (2007) 8–16.
[35] B.C. Wonsiewi, W.A. Backofen, Plasticity of magnesium crystals, Trans. Metall. Soc. AIME 239 (1967) 1422–1431.